PHYSICAL REVIEW B **80**, 245432 (2009)

Transition from ballistic to diffusive behavior of graphene ribbons in the presence of warping and charged impurities

J. W. Klos,[1,2,*] A. A. Shylau,[2] I. V. Zozoulenko,[2,†] Hengyi Xu,[3] and T. Heinzel[3]
[1]*Surface Physics Division, Faculty of Physics, Adam Mickiewicz University, Umultowska 85, 61-614 Poznań, Poland*
[2]*Solid State Electronics, Department of Science and Technology, Linköping University, 601 74 Norrköping, Sweden*
[3]*Condensed Matter Physics Laboratory, Heinrich-Heine-Universität, Universitätsstrasse 1, 40225 Düsseldorf, Germany*

(Received 28 August 2009; revised manuscript received 23 November 2009; published 22 December 2009)

We study the effects of the long-range disorder potential and warping on the conductivity and mobility of graphene ribbons using the Landauer formalism and the tight-binding p-orbital Hamiltonian. We demonstrate that as the length of the structure increases the system undergoes a transition from the ballistic to the diffusive regime. This is reflected in the calculated electron-density dependencies of the conductivity and the mobility. In particular, we show that the mobility of graphene ribbons varies as $\mu(n) \sim n^{-\lambda}$, with $0 \leq \lambda \lesssim 0.5$. The exponent λ depends on the length of the system with $\lambda = 0.5$ corresponding to short structures in the ballistic regime, whereas the diffusive regime $\lambda = 0$ (when the mobility is independent on the electron density) is reached for sufficiently long structures. Our results can be used for the interpretation of experimental data when the value of λ can be used to distinguish the transport regime of the system (i.e., ballistic, quasiballistic, or diffusive). Based on our findings we discuss available experimental results.

DOI: 10.1103/PhysRevB.80.245432 PACS number(s): 73.63.−b, 72.10.−d, 73.23.Ad

I. INTRODUCTION

The two-dimensional allotrope of carbon graphene has become a subject of intensive research since its isolation in 2004.[1] This is because of its fundamental significance, its unusual electronic properties, as well as its potential for numerous applications (for a review see, e.g., Ref. [2]).

A very interesting and not fully resolved problem is the impact of various mechanisms such as disorder, substrate, environment, etc., on the transport properties of graphene. Particular attention has been devoted to studies of the effect of charged impurities (located in the substrate or on its surface) which is widely considered to be the main mechanism limiting the mobility in graphene.[3–8] Indeed, recent experiments on suspended graphene sheets have demonstrated a significant improvement of electrical transport in suspended devices compared to traditional samples where the graphene is supported by an insulating substrate.[9,10]

Another important mechanism that can affect the transport in graphene is warping, when the graphene, as an elastic membrane, tends to become rippled in order to minimize the elastic energy.[11–18] The warped character of a graphene surface has been proved in diffraction experiments[11] and scanning tunnel microscope measurements[17,18] for both suspended samples and samples on an insulating substrate. It has been demonstrated that due to the rehybridization effects and the change in the next-to-nearest-neighbor hopping integrals caused by curvature the warping generates spatially varying potential that is proportional to the square of the local curvature.[13]

The transport properties of the graphene can also be strongly affected by its interaction with the substrate and other materials which may exist in its environment.[19] This includes, e.g., the interaction of the graphene with the surface polar modes of SiO_2 or with water molecules that might reside on the surface. These interactions have a long-range character and because of the corrugated character of the graphene and/or dielectric surfaces, the spatial variation in these interactions would result in a spatially varying effective potential affecting the transport properties of the graphene sheet.

The purpose of the present paper is twofold. Our first aim is to study the effect of warping on the transport properties of graphene ribbons. The warping of the graphene affects both the nearest-neighbor and the next-to-nearest-neighbor hopping integrals, t and t', respectively. Previous works dealt primarily with the effect of the modification of the next-to-nearest-neighbor hopping integrals.[13,16] This is because the next-to-nearest-neighbor hopping integrals t' are much more strongly affected by out-of-plane deformations in comparison to the nearest-neighbor integrals t. On the other hand, because the electronic and transport properties of graphene are primarily determined by the nearest-neighbor hopping, it is not *a priori* clear which effect is dominant. In this work we, based on the realistic model of a warped graphene surface and the tight-binding p-orbital Hamiltonian, numerically study the effect of modification of the nearest-neighbor hopping integrals t on the conductance of the graphene ribbons. We find that the modification of the nearest-neighbor hopping integrals due to the out-of-plane deformations of the graphene surface has a negligible effect on the conductance in comparison to the effect of charged impurities even for moderate strength and concentration.

The second and main aim of our study is the investigation of the transition from the ballistic to the diffusive behavior of graphene ribbons with a realistic long-range disordered potential. One of the motivations for this study is recent experiments addressing the mobility of suspended and nonsuspended graphene devices of submicrometer dimensions. The dimension of these devices is smaller than the phase coherence length l_ϕ at the low temperature ($l_\phi \sim 3-5$ μm at 0.25 K and ~ 1 μm at 1 K) (Refs. [20] and [21]) and the mean-free path (mfp) approaches its ballistic value.[10] This indicates that these submicrometer devices can be in the quasiballistic and even ballistic transport regime requiring the Landauer approach for the description of the transport. At the same time, the electron transport in these devices was analyzed in terms of the classical mobility μ which is appropriate for a diffusive transport regime. In the present study we use a realistic model of a disordered potential and the tight-binding p-orbital Hamiltonian, and perform numerical calculations of the conductance of graphene ribbons based on the Landauer formalism. We demonstrate that as the size of the system L increases the system undergoes a transition from the ballistic to the diffusive regime. This is reflected in the calculated electron-density dependence of the conductivity and the mobility. In particular, we show that the mobility of graphene ribbons varies as $\mu(n) \sim n^{-\lambda}$, with $0 \leq \lambda \lesssim 0.5$. The exponent λ depends on the size of the system with $\lambda = 0.5$ corresponding to short structures in the purely ballistic regime, whereas the diffusive regime corresponds to $\lambda = 0$ (when the mobility is independent on the electron density) and is reached for sufficiently long structures. Our results can be used for the interpretation of experimental data when the value of the parameter λ can distinguish the transport regime of the system (i.e., ballistic, quasiballistic, or diffusive).

It should be noted that various aspects of the effect of the disorder on the electron transport in graphene have been extensively studied in the past.[22–35] We stress that the focus of our study is the understanding of the transition from the ballistic to the diffusive regime when the obtained electron-density dependencies of the conductivity and the mobility can be used to extract information on the character of the transport regime of the system at hand. Note that in contrast to many previous studies focusing on the metal-insulator transition and the strong localization regime, in the present paper we consider the case of a ribbon with many propagating channels when the localization length exceeds the size of the system.

Finally, it is well established that edge disorder strongly affects the transport properties of graphene ribbon.[22–33,36,37] However, the measurements of the mobility are typically done in the multiterminal Hall geometry where the edges do not play a role. Therefore, in the present study we consider perfect edges to make sure that the electron conductance is influenced only by the long-range potential in the bulk. In our calculations we use the long-range potential corresponding to remote charged impurities. We however demonstrate that the obtained results are not particularly sensitive to the parameters of the potential. We therefore can expect that our findings can be applicable not only to the charged impurities but to other mechanisms discussed above (e.g., interaction with the surface polar modes, etc.) that can also be described by a similar long-range potential.

The paper is organized as follows. In Sec. II A we present the basics of our computational method for calculation of the conductance and the mobility of graphene ribbons. The models of warping and remote impurities are described in Secs. II B and II C. The conductivity and the mobility of graphene ribbons in the presence of warping and charged impurities are presented and discussed in Sec. III. Section IV contains the summary and conclusions.

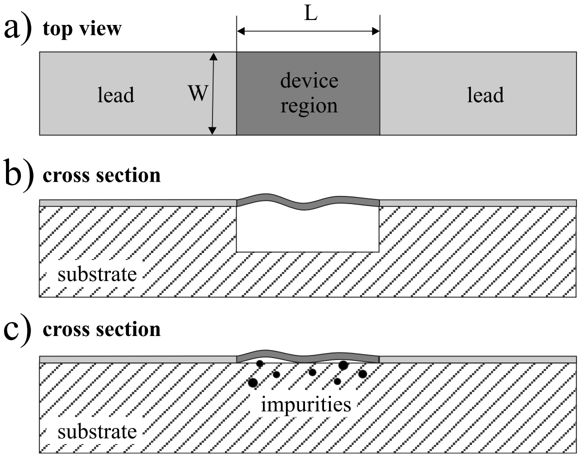

FIG. 1. The schematic sketch presenting the structure under consideration: (a) top view of the device region (dark gray area) attached to the semi-infinite graphene leads (light gray areas), (b) free standing, rippled graphene layer, and (c) graphene layer supported on the substrate (white area) in the presence of charged impurities (dots).

II. MODEL

A. Basics

In order to describe transport and electronic properties of graphene we use the standard p-orbital tight-binding Hamiltonian,

$$H = \sum_i V_i |i\rangle\langle i| - \sum_{i,j} t_{i,j} |i\rangle\langle j| \tag{1}$$

limited to the nearest-neighbor hopping. V_i denotes the external potential at the site i; the summation of i runs over the entire lattice while j is restricted to the sites next to i. We relate the spatial variation in the hopping integral $t_{i,j}$ with bending and stretching of the graphene layer due to warping as described in the next section.

The conductance G and the electron density n are computed with the aid of the recursive Green's function technique.[38,39] We assume that the semi-infinite leads are perfect graphene ribbons, and the device region is a rectangular graphene strip and the imperfections (warping and long-range impurity potential) are restricted only to this area (see Fig. 1). The zero-temperature conductance G is given by the Landauer formula

$$G = \frac{2e^2}{h} T, \tag{2}$$

where T is the total transmission coefficient between the leads. Then we calculated the conductivity

$$\sigma = \frac{L}{W} G, \tag{3}$$

the electron density

$$n(E) = \int_0^E dE \;\mathrm{DOS}(E), \tag{4}$$

the mobility

$$\mu = \frac{\sigma}{en}, \tag{5}$$

and the mfp

$$\mathrm{mfp} = \frac{h}{2e^2}\frac{\sigma}{\sqrt{\pi n}}, \tag{6}$$

as functions of the Fermi energy E (W and L denote width and length of device, respectively). The density of states (DOS) was computed by averaging the local density of states (LDOS) over the whole device area. The LDOS is given by the diagonal elements of the total Green's function.[39]

All the results presented here correspond to the ribbons of the zigzag orientation. Previous studies do not show a difference of the transport properties of the zigzag and armchair ribbons in the presence of disorder (provided the disorder concentration is sufficiently high).[30,33,37] Even in the ballistic regime the overall dependencies $n=n(E)$ and $\sigma=\sigma(E)$ are qualitatively the same for both orientations (see Appendix). We therefore expect that all the results reported here remain valid for the case of the armchair orientation as well.

The effect of warping is included in our model by modification of hopping integrals t resulting from stretching (contraction) and π-σ rehybridization. The external potential of remote impurities (with inclusion the effect of screening by carries) is reflected in the model by changing of site energies. In the next section we present a detailed description of models for the warping and remote impurities.

B. Corrugation

The mechanical properties of graphene can be modeled by treating this system as an elastic membrane. One can distinguish two modes of deformation: stretching/contraction and bending. Both of them affect the strength of carbon-carbon (C-C) bonds within the graphene sheet by changing the distance between carbon atoms and the alignment of their p orbitals, respectively. In the tight-binding model the hopping integral corresponding to the hybridized σ-π bond is given by[40,41]

$$\begin{aligned} t(a,\theta,\phi,\vartheta) &= \cos(\vartheta)\cos(\theta)\cos(\phi)t_{2p\pi,2p\pi}(a) \\ &\quad - \sin(\vartheta)\sin(\theta)t_{2p\sigma,2p\sigma}(a), \\ t_{2p\pi,2p\pi}(a) &= \alpha_\pi e^{a\zeta}\left[1 + a\zeta + \frac{2}{5}(r\zeta)^2 + \frac{1}{15}(r\zeta)^3\right], \\ t_{2p\sigma,2p\sigma}(a) &= \alpha_\sigma e^{a\zeta}\left[-1 - a\zeta - \frac{1}{5}(a\zeta)^2 + \frac{2}{15}(a\zeta)^3\right], \end{aligned} \tag{7}$$

where $\alpha_\pi/t_0 \approx -4.23$, $\alpha_\sigma/t_0 \approx -4.33$, and $\zeta \approx 3.07$ Å^{-1} ($t_0 = 2.7$ eV and $a_0 = 1.42$ Å) are the hopping integral and the C-C bond length for flat ($\theta=0, \phi=0, \vartheta=0$) and unstrained ($a=a_0$) graphene ribbon, respectively. $t_{2p\pi,2p\pi}$ and $t_{2p\sigma,2p\sigma}$ denote the hopping integrals for pure π bonds (in flat graphene) and σ bonds (for collinear p orbitals). The spatial orientation of the p orbitals is described by the angles θ, ϕ, ϑ as presented in Fig. 2.

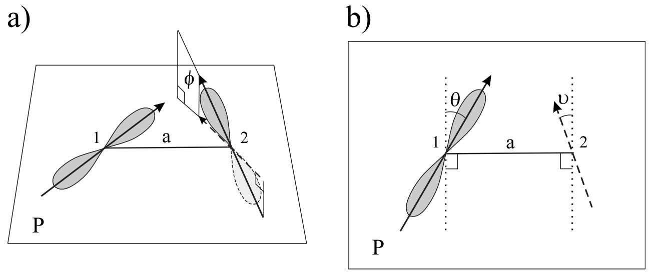

FIG. 2. Definition of angles [used in Eq. (7)] describing alignment of p orbitals of neighboring atoms; the symbol a denotes the bond length. (a) ϕ denotes the angle between direction of orbital 2 and its projection (dashed arrow) on the plane P spanned on the direction of the orbital 1 and the vector linking the centers of the orbitals 1 and 2. (b) Top view of the plane P. All vectors depicted here belong to the plane P and have the same meaning as in (a). Dotted lines are perpendicular to the vector linking centers of the orbitals 1 and 2. Note that in the panel (b) the orbital 2 is not shown.

The analysis of diffraction patterns of corrugated graphene[11] provides information about the range in which the normal to the surface varies. The measured range ±5° allows to estimate from Eq. (7) an impact of bending on the relative change in the hopping integral, $[t(a_0,\theta,\phi,\vartheta) - t_0]/t_0 \approx 0.4\%$. The information about the distribution of bond lengths in corrugated graphene is provided by the Monte Carlo simulations.[12] Using these data we can calculate the change in hopping integrals [Eq. (7)]. The relative change in the hopping integral for $\theta=\phi=\vartheta=0$ and C-C bond variation $\Delta a = a - a_0$, corresponding to the half width at half height (HWHH) of the bond-length distribution,[12] is approximately $[t(a) - t_0]/t_0 \approx 2\%$. This comparison shows that the effect of strain (leading to a change in the bond length Δa) has a stronger impact on the modification of the hopping integrals in comparison to the effect of bending (related to the orbital alignment).

In a corrugated free standing membrane the bending and the in-plane strain are related to each other.[42–44] For example, in order to produce a local minimum/maximum or a saddlelike area in a flat membrane it is necessary to introduce a strain (see Fig. 3). Bending and strain of the free standing membrane can be related to the Gauss curvature,

$$c_G(x,y) = c_1(x,y)c_2(x,y), \tag{8}$$

which is the product of the minimum c_1 and maximum c_2 of normal curvatures[45] (called by principal curvatures). The curvatures c_1 and c_2 are given by the inverse radiuses of the local curvatures, $|c_1| = 1/R_1$ and $|c_2| = 1/R_2$, see Fig. 3. The sign of c_1 and c_2 depends on whether an intersection of the normal plane with the surface is convex or concave. The positive value of c_G at some point corresponds to a local minimum/maximum which requires stretching of this region. For a saddlelike area (and negative value of c_G) the local

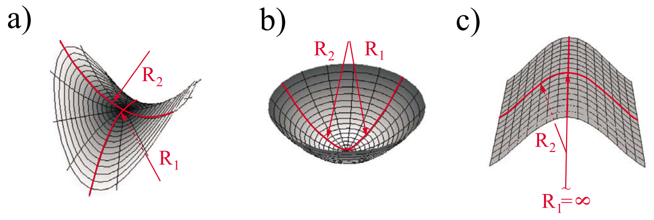

FIG. 3. (Color online) (a) A saddlelike surface and (b) a local minimum created by a nonuniform contraction (dark areas) and inflation (light areas) of a flat region. (c) Developable surface (i.e., the surface with zero Gauss curvature). Each red curve and the vectors showing the radius of curvature lie in the same normal plane.

contraction of a flat membrane is needed. The only kind of bending which does not produce strain corresponds to developable surfaces (i.e., surfaces with zero Gauss curvature) such as, e.g., a cylindrical tube, see Fig. 3(c).

Because of a small variation in the relative change in the bond length $\Delta a/a_0$ we assume a linear dependence of the bond elongation/contraction Δa on the Gauss curvature,

$$\Delta a(x,y) = k c_G(x,y). \tag{9}$$

The value of the coefficient k was chosen to reproduce the range of the Δa variation computed by Fasolino *et al.*[12] We estimated the HWHH of Δa from the C-C bond-length distribution presented in Ref. 12. Then, we computed the HWHH of c_G distribution for a large (generated as described below) corrugated ribbon. The coefficient k was defined as the ratio of the HWHHs for the Δa and c_G distributions.

In our model we do not take into account an influence of the surface corrugation on the position of carbon atoms. The positions of the centers of C-C bonds in flat lattice were projected onto a corrugated continuous surface. In these points the Gauss curvature was computed. The value of c_G was used to calculate the change in the bond lengths [Eq. (9)]. The angles θ, ϕ, ϑ (see Fig. 2) were calculated from the alignment of normals representing the π orbitals. The normals were computed at the ends of the projected bonds. The computed angles θ, ϕ, ϑ and C-C bond lengths $a = a_0 + \Delta a$ were used to calculate the next-neighbor hopping integrals [Eq. (7)] in the corrugated ribbon.

In order to model the geometry of a corrugated ribbon we used the description of fluctuations of elastic membranes presented in Ref. 12. The ripples on the graphene surface can be expanded as a Fourier series of plane waves characterized by the wave vectors $\boldsymbol{q}$. In the harmonic approximation[12] the in-plane and out-of-plane displacement h are decoupled. In this approximation the mean-square amplitude of Fourier component h_q is given by[14,43]

$$\langle h_q^2 \rangle \sim \frac{1}{q^4}. \tag{10}$$

It can be shown that the mean square of the out-of-plane displacement h scales quadratically with the linear size of the sample,[12]

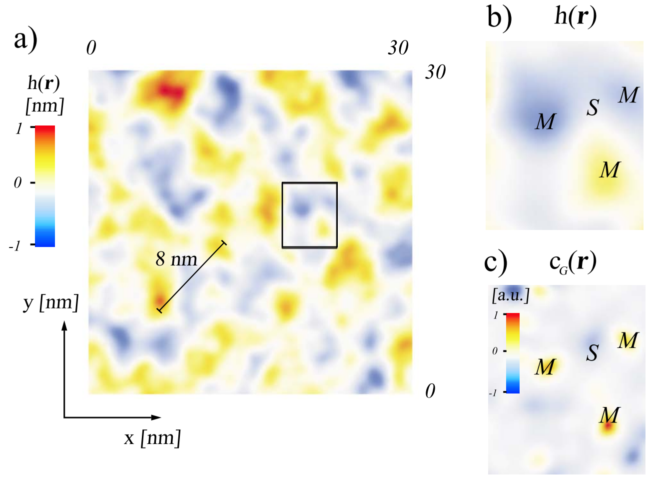

FIG. 4. (Color online) The model of ripples on the graphene surface. The black lines denote characteristic length of ripples 8 nm; (b) the magnified small area marked in (a) by a black frame; M and S stand for local maxima (minima) and saddle points, respectively; (c) the Gauss curvature corresponding to a part of the surface presented in (b)—red/orange (blue) areas mark regions with positive (negative) Gauss curvature.

$$\langle h^2 \rangle = \sum_q \langle h_q^2 \rangle \sim L^2. \tag{11}$$

According to Eq. (11) the height of the ripples increases quadratically with the sample size. It means that a large sample should be crumpled ($\langle h^2 \rangle \gtrsim L$) which contradicts the experiments. The results consistent with the experiments where large sample remains approximately flat are reproduced by the Monte Carlo simulations[12] where the dependence $\langle h_q^2 \rangle \sim q^{-4}$ [Eq. (10)] remains valid for short wavelengths only and saturates for the long wavelengths $\lambda = 2\pi/q \gtrsim \lambda^* \approx 8$ nm. This mechanism is responsible for the existence of ripples of characteristic size $\sim\lambda^*$, see Fig. 4.

Using this guidance we modeled the corrugated surface in the following way. The surface $h(\boldsymbol{r})$ was generated by a superposition of plane waves,

$$h(\boldsymbol{r}) = C \sum_i C_{q_i} \sin(\boldsymbol{q}_i \cdot \boldsymbol{r} + \delta_i), \tag{12}$$

where $\boldsymbol{r} = (x_1, x_2)$ is the in-plane position vector. The directions φ_i of the wave vectors $\boldsymbol{q}_i = q_i[\cos(\varphi_i), \sin(\varphi_i)]$ and the phases δ_i were chosen randomly. The length of wave vectors q_i covers equidistantly the range $2\pi/L < q_i < 2\pi/(3a_0)$, where L is a leading linear size of the rectangular area and a_0 denotes the C-C bond length (we assume that $L \gg \lambda^*$). The amplitude of the mode was given by the harmonic approximation [Eq. (10)] $C_q = \sqrt{2\langle h_q^2 \rangle}$ for the wavelength $\lambda < \lambda^*$, otherwise it was kept constant and equal to C_{q^*}, where $q^* = 2\pi/\lambda^*$. We introduced the normalization constant C to keep the averaged amplitude of the out-of-plane displacement $\bar{h} = \sqrt{2\langle h^2 \rangle}$ equal to the experimental values $\bar{h} \approx 1$ nm for typical sizes of samples.

In Fig. 4 the graphene surface, generated by using the procedure described above, is shown. Long-wave ripples of the size $\sim\lambda^* \approx 8$ nm discussed above are clearly seen. A small area marked in a box in Fig. 4(a) is enlarged in Fig. 4(b). In this region two minima (blue spots), one maximum (yellow spot) and one saddle region (white area between color spots) are shown. The relation between the geometry of the surface and its Gauss curvature can be visible in Fig. 4(c). The regions of stretching (red and yellow spots) and contraction (blue spot) in Fig. 4(c) correspond to the position of minima/maximum (M) and saddle area (S) in Fig. 4(b), respectively.

C. Long-range potential

A long-range character of the electrostatic interaction is included in the model of bare Coulomb-type scattering centers,

$$V_i = \frac{1}{4\pi\epsilon_r\epsilon_0} \sum_{i'=1}^{N_{imp}} \frac{e^2}{|\boldsymbol{r}_i - \boldsymbol{r}_{i'}|}, \tag{13}$$

where ϵ_0 and ϵ_r stand, respectively, for the vacuum and relative permittivities. For this potential the conductivity is proportional to electron density, $\sigma \sim n/n_{imp}$.[7] However, the application of the bare Coulomb potential can be justified only for low values of the electron density when the screening effects limiting the range of the potential are negligible.

The simplest screened potential is given by the Thomas-Fermi approximation,[46]

$$V_i = U_{TF} \sum_{i'=1}^{N_{imp}} \frac{\exp(-\xi_{TF}|\boldsymbol{r} - \boldsymbol{r}_i|)}{|\boldsymbol{r}_i - \boldsymbol{r}_{i'}|}, \tag{14}$$

where the parameters U_{TF} and ξ_{TF} describe the strength and the range of the scattering centers for the Thomas-Fermi potential. The inclusion of screening allows to achieve both the limits of Coulomb scattering (for low n) and short-range scattering (for high n).

The singularity at $\boldsymbol{r}_i = \boldsymbol{r}_{i'}$ in the Thomas-Fermi potential [Eq. (14)] can cause numerical difficulties. In our calculation we utilize a model for screened scattering centers of the Gaussian shape commonly used in the literature where the potential on the site i reads[22,23,31]

$$V_i = \sum_{i'=1}^{N_{imp}} U_{i'} \exp\left(-\frac{|\boldsymbol{r}_i - \boldsymbol{r}_{i'}|^2}{2\xi^2}\right), \tag{15}$$

where the height of scattering centers is uniformly distributed in the range $U_{i'} \in [-\delta, \delta]$, see Fig. 5 for illustration. The strength and correlation between the scattering centers is described by the dimensionless correlator K,[23,31]

$$\langle V_i V_j \rangle = \frac{K(\hbar v_F)^2}{2\pi\xi^2} \exp\left(-\frac{|\boldsymbol{r}_i - \boldsymbol{r}_j|^2}{2\xi^2}\right), \tag{16}$$

(note that $\langle V_i \rangle = 0$). The averaging is preformed for all possible configurations of system which differ only in the distribution of the position of the impurities $\boldsymbol{r}_{i'}$ and the strength $U_{i'}$ (δ, ξ, and n_{imp} are kept constant).

For this impurity potential both the screening range ξ and the impurity strength δ are independent on the electron density and play the role of parameters. They are related to K by following formula:[23]

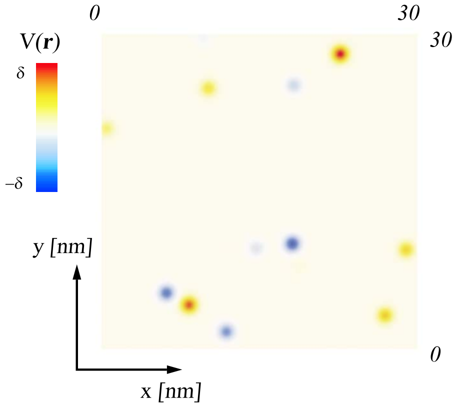

FIG. 5. (Color online) Illustration of the long-range potential, Eq. (15). The screening range is $\xi = 4a_0$ and the impurity concentration is $n_{imp} = 10^{12}$ cm^{-2}.

$$K \approx 40.5\tilde{n}_{imp}(\delta/t)^2(\xi/a_0), \tag{17}$$

where $\tilde{n}_{imp} = N_{imp}/N$ denotes the relative concentration expressed via the total number of impurities N_{imp} and the atomic sites N in a sample. In our calculation we use $n_{imp} = 10^{12}$ cm^{-2} as a typical value given in the experiment.[10] We assumed that the screening range $\xi = 4a_0$. The strength of impurities was chosen in order to get typical values of correlator[6,22] (we chose $K = 1, 2, 4, 8$).

III. RESULTS AND DISCUSSION

Let us start with the comparison of the effects of warping and charged impurities on the conductance of a graphene ribbon. Figure 6 shows the conductances of a ribbon with warping and flat ribbons with two representative impurity concentrations $n_{imp} = 10^{12}$ and 4×10^{12} cm^{-2} (dashed and dotted lines, respectively). The warping modifies the conductance only slightly. For low energies close to the charge neutrality point the conductance steps remain practically unaffected. For higher energies the conductance steps become somehow distorted with the conductance plateaus being gradually shifted down and sharp minima appearing next to the rising edges of the plateaus. At the same time, in the presence of charged impurities even of a moderate strength the conductance of the ribbon is distorted substantially. The conductance steps are significantly washed out and the overall slope of the curve is lowered.

Our results thus demonstrate that the modification of the nearest-neighbor hopping integrals t resulting from stretching (contraction) and π-σ rehybridization has only a small effect on the conductance in comparison to the effect of impurities. It should be also noted that the effect of the modification of the next-to-nearest hopping integrals t' is also weak in comparison to a realistic impurity potential. For example, Kim and Castro Neto[13] estimated that the variation in the effective electrochemical potential generated by a spatial variation in t' is on the order of 30 meV, which is an order of magnitude smaller than a corresponding variation in the im-

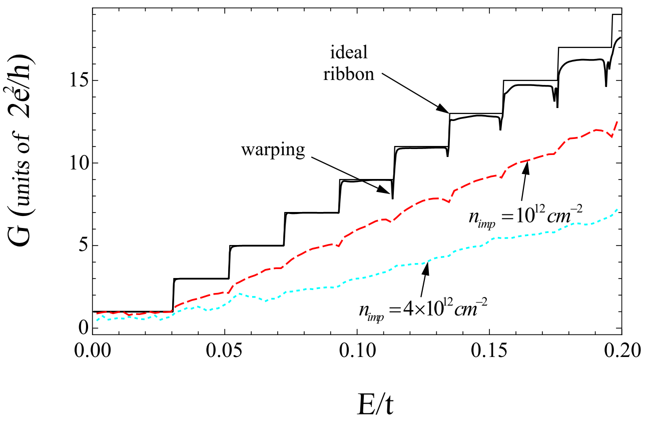

FIG. 6. (Color online) Effect of warping and charged impurities on the conductance of graphene nanoribbon of length $L=30.6$ nm and width $W=31.8$ nm (250×150 sites). The thin line shows the conductance steps for an ideal ribbon. The bold line denotes the conductance for a system with warping only; dashed and dotted lines refer to the conductance of a ribbon with impurities (without warping) with the concentration $n_{imp}=10^{12}$ cm^{-2} and 4×10^{12} cm^{-2}, respectively, averaged over ten impurity configurations. The strength of the impurities is $\xi=4a$ and $K=2$. The inset shows an enhanced view of the conductance in the vicinity of the first conductance step.

purity potential.[3,31] Hence, in our further analysis of the conductivity and the mobility of graphene ribbons we will take into to account the impact of charged impurities only.

Let us now turn to the investigation of transition from the ballistic to diffusive regime of transport taking place as the size of the system increases. Because of computational limitations we keep in our study the width of the ribbon W constant and increase its length L, such that the diffusive regime is achieved when $L/W\gg1$. We however demonstrate below that the presented results and conclusions remain valid even for bulk diffusive samples with the aspect ratio $L/W\sim1$.

Figure 7 shows the conductivity σ of ideal ballistic graphene ribbons of different lengths L exhibiting a linear dependence on the electron energy E. This behavior reflects the corresponding linear dependence of the conductance G of zigzag ribbons as a function of energy (see Appendix for details). Note that the conductance of an ideal ribbon in the ballistic regime is independent on the length of the system. Therefore, for fixed energy, the conductivity $\sigma=\frac{L}{W}G$ increases linearly with the ribbon length L as illustrated in Fig. 7(c). Apparently, in the ballistic regime, the conductivity does not exist as a local property and cannot be considered as material parameter because it is size dependent.

The conductivity of the ribbons of different lengths as a function of the electron energy in the presence of impurities is shown in Fig. 7(b). The conductivity is strongly reduced in comparison to the ideal conductance steps and is no longer a linear function of the electron energy. Instead, it follows a power-law dependence

$$\sigma\sim E^{\alpha}, \tag{18}$$

where the exponent α approaches $\alpha=2$ for sufficiently long ribbons [see inset of Fig. 7(b)]. Figure 7(c) shows the depen-

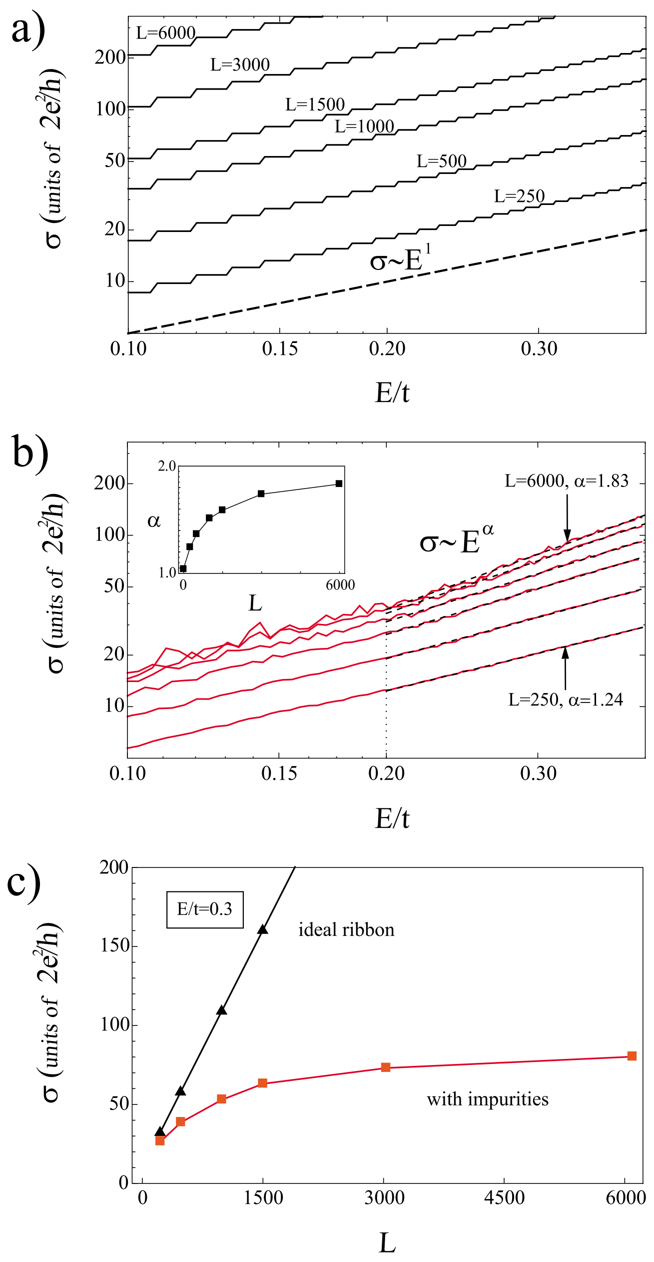

FIG. 7. (Color online) (a) The conductivity of (a) ideal ballistic nanoribbons and (b) nanoribbons with impurities as a function of the Fermi energy E. The nanoribbon lengths are $L=31$, 61, 123, 184, 369, and 738 nm corresponding to 250, 500, 1000, 1500, 3000, and 6000 sites. The conductivities in (b) are averaged over ten impurities configuration. The dashed lines show the fit $\sigma\sim E^{\alpha}$ for the energies $E>0.2t$ as indicated by a vertical dotted line. (Here and hereafter we choose $E>0.2t$ because for lower energies the fitted dependencies deviate from the power-law behavior due to sample-specific fluctuations). The inset shows a dependence $\alpha=\alpha(L)$. The impurity parameters are $n_{imp}=10^{12}$ cm^{-2}, $K=2$, and $\xi=4a$. (c) The conductivity as a function of the ribbon length L for ballistic ribbons and ribbons with impurities. The ribbon width is $W=53.1$ nm (250 sites). (Note that for the zigzag ribbons the same number of sites in the x and y directions corresponds to somehow different dimensions, e.g., 250×250 sites corresponds to 31×53 nm^2.)

dence of the conductivity σ on the length of the system in the presence of impurities. This dependence exhibits a clear saturation of the conductivity for sufficiently large systems, $L \gtrsim 6000$ sites (740 nm). In order to understand these features, in particular, the dependence of the conductivity on the system size L, let us recall that the conductance of a disordered system is expected to obey the scaling law

$$\ln(1 + 1/g) = L/\xi_{loc}, \tag{19}$$

where ξ_{loc} is the localization length and $g = G/G_0$ is the dimensionless conductance ($G_0 = 2e^2/h$ being the conductance unit).[47] In this study we focus on the transport regime with many transmitted channels $g \gg 1$. It follows from Eq. (19) that this corresponds to the case $\xi_{loc} \gg L$, i.e., the localization length exceeds the size of the system and the conductance is inversely proportional to the length, $G \sim G_0/L$. In this transport regime referred to as a diffusive (or Ohmic), the conductivity σ is therefore independent on the system size and can be regarded as a local quantity. According to Fig. 7(c) this transport regime is achieved for sufficiently long ribbons, $L \gtrsim 6000$ sites (740 nm). For smaller L the system is in a quasiballistic regime when the conductivity σ depends on the size of the system. In this case the conductance G is apparently more appropriate quantity to describe the transport properties of the system at hand.

Let us now turn to the analysis of the mobility of graphene ribbons μ. For a classical (Ohmic) conductor the mobility is the fundamental material property independent on the system size and the electron density. In contrast, for ballistic ribbons the mobility is size dependent and decreases with increase in the electron density as $\mu \sim n^{-0.5}$ (see Appendix). Therefore one can expect that the mobility of ribbons varies as

$$\mu(n) \sim n^{-\lambda}, \tag{20}$$

where the exponent λ ranges from 0 in the diffusive limit to 0.5 in the ballistic limit.

In order to calculate the electron mobility $\mu = \sigma/en$ we, in addition to the conductivity σ, have to calculate the electron density n in the ribbons (note that this step represents the most time-consuming part of our numerical calculations because in order to calculate n we have to compute the DOS for all energies $0 < E < E_F$). Figure 8 shows the DOS for a representative impurity configuration and electron densities for ribbons of different lengths calculated from the DOS according to Eq. (4). For ideal ribbons, the DOS follows an overall linear dependence on the energy with the singularities corresponding to openings of new propagating channels characteristic for quasi-one-dimensional systems. Because of this linear increase in the DOS, the electron density for an ideal ribbon follows a quadratic dependence on the energy, $n \sim E^2$ (see Appendix). Figure 8(a) shows that the impurities only smear out the singularities in the DOS of an ideal ribbon but do not reduce the DOS. Therefore, regardless of the ribbon lengths the average electron density in the ribbons with impurities is not reduced in comparison to the ideal ribbons and follows the same quadratic dependence $n \sim E^2$. This behavior is expected for the transport regime at hand when the localization length exceeds the size of the system, $\xi_{loc} \gg L$, such that the averaged LDOS is essentially independent of the size of the system. Note that in the opposite regime of the strong localization, $\xi_{loc} \ll L$, the electron density in ribbons is strongly reduced due to the effect of impurities.[33]

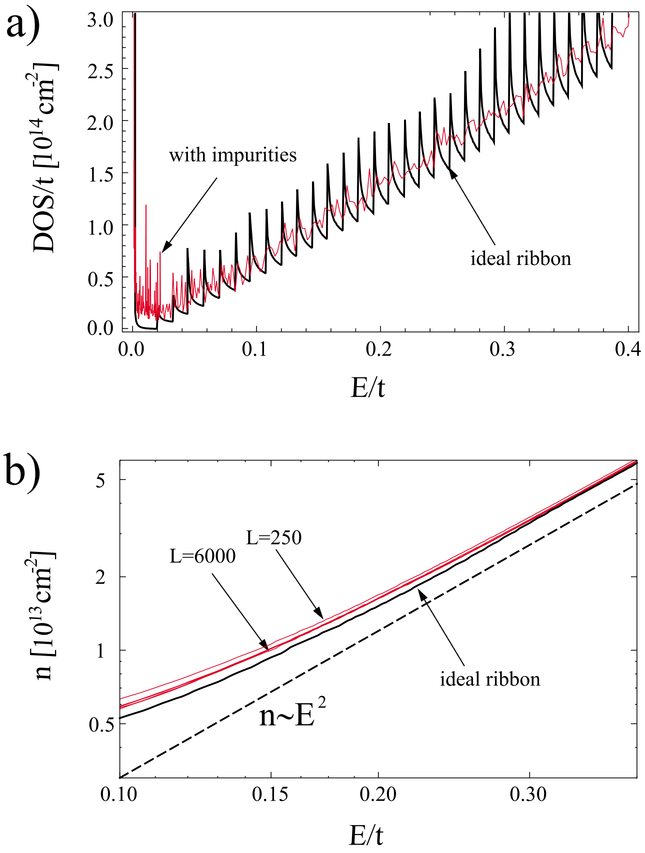

FIG. 8. (Color online) (a) The DOS as a function of the Fermi energy of an ideal ribbon (solid line) and of a ribbon of the length $L = 184$ nm (1500 sites) for a representative impurity configuration. (b) The dependence of the electron density n on the Fermi energy for an ideal ribbon and for ribbons of various length with impurities. The parameters of the ribbons and the impurity strength are the same as in Fig. 7. (Note that the electron densities for the ribbons with the length $L > 250$ sites are almost indistinguishable).

For low energies close to the charge neutrality point $E = 0$ the DOS of the system with impurities shows sharps peaks whose positions are strongly system dependent, see Fig. 8(a). This is because in this energy interval the system is in the strong localization regime with the localization length being smaller than the system size (for an analysis of this transport regime see Ref. 33). In this energy interval the DOS is strongly system dependent because it reflects a particular configuration of the impurity potential. This explains some differences in the electron densities for different ribbons in Fig. 8(b) (especially for the shortest one with $L = 250$ sites) because the integration in Eq. (4) includes all the energies (below Fermi energy), including those close to $E = 0$ where the DOS can show strong system-specific fluctuations.

Having calculated the electron density and the conductivity, we are in a position to discuss the mobility of the system at hand. The mobility of the ideal ribbons of different lengths L as a function of the electron density is shown in Fig. 9(a). This corresponds to the ballistic regime with $\lambda=0.5$. For a given electron density the mobility of the ballistic ribbons is proportional to the ribbon length, $\mu \sim L$ [because $\mu=\sigma/en$ and $\sigma \sim L$, see Fig. 7(c)].

Let us now investigate how the mobility of a ribbon evolves as we go from the quasiballistic to the diffusive regime by increasing the system size. Figure 9(b) shows the mobility of the ribbon with impurities as a function of the electron density. As expected, this dependence satisfies Eq. (20). The dependence $\lambda=\lambda(L)$ is shown in the inset of Fig. 9(b). This dependence clearly demonstrates that we approach the diffusive regime (with the expected value of $\lambda=0$) as the length of the ribbons becomes sufficiently long ($L \gtrsim 740$ nm). This is fully consistent with the behavior of the conductivity discussed above which exhibits a transition to the diffusive transport regime as the length of the ribbon increases.

The calculated dependence $\lambda=\lambda(L)$ is also consistent with the energy dependence of the conductivity which approaches the quadratic behavior $\sigma \sim E^2$ in the diffusive regime [see inset of Fig. 7(b)]. Because $n \sim E^2$ regardless of the regime (ballistic, quasiballistic, or diffusive), the mobility $\mu=\sigma/en$ becomes independent on the energy (and thus on the electron density with $\lambda=0$) only when $\sigma \sim E^2$. To illustrate this we in Fig. 9(c) present the dependence $\sigma=\sigma(n)$ which is plotted by combining previously calculated dependencies $\sigma=\sigma(E)$ and $n=n(E)$. As expected from Eqs. (5) and (20) it follow a dependence

$$\sigma(n) \sim n^{\gamma}, \tag{21}$$

where the exponent γ ranges from 1 in the diffusive limit to 0.5 in the ballistic limit.

A crossover from the ballistic to the diffusive regime is also manifested itself in the behavior of the mean-free path [Eq. (6)]. Based on Eq. (21) the density dependence of the mfp can be presented in the form

$$\text{mfp}(n) \sim n^{\epsilon}, \tag{22}$$

where the exponent ϵ ranges form 0 (ballistic limit) to 0.5 (diffusive limit). Figure 9(d) shows the dependence mfp $=\text{mfp}(n)$ for ribbons of different lengths and the inset of Fig. 9(d) illustrates the expected dependence given by Eq. (22), where $\epsilon=0$ corresponds to short ribbons in the ballistic regime, whereas $\epsilon=0.5$ is approached for long diffusive ribbons. It is worth to stress that in the ballistic regime mfp is larger than the width of the ribbons, whereas for longer ribbons the mfp is smaller (or comparable) to their length.

All the results for the conductivity, electron density, the mobility, and mfp in the graphene ribbons presented above correspond to the case of one representative impurity strength $n_{imp}=10^{12}$ cm^{-2}, $K=2$, and $\xi=4a$. It is important to stress that the scaling laws discussed above are rather insensitive to a particular realization of the potential configuration or the impurity strength provided that the system is in the transport regime when the localization length is larger than the ribbon size. This is illustrated in Fig. 10 showing the conductivity, the electron density and the mobility in graphene ribbons for different impurity strength $K=1,2,4,8$. As expected, the electron density is similar for all ribbons, especially for high energies, see Fig. 10(b). When the impurity strength increases the conductivity apparently decreases, see Fig. 10(a). This decrease in the conductivity leads also to the decrease in the mobility as shown in Fig. 10(c). However, the exponents in the scaling laws [Eqs. (18) and (19)] are not particularly sensitive to the variation in the impurity strength K. A small difference in scaling exponents for different impurity strengths has a statistical origin and this difference diminishes as a number of impurity configurations used in calculations of each curve is increased.

Because of computational limitations the diffusive limit in our calculations was reached by the increase in the length of nanoribbons keeping their width constant. Because of this reason most of the reported results correspond to the ribbons with a small aspect ratio $W/L \ll 1$. Do the obtained results remain valid for relatively wide ribbons with the aspect ratio $W/L \sim 1$? In order to check this we fix the ribbon's length L and increase its width W approaching the aspect ratio $W/L \sim 1$. Figure 11 shows the calculated mobilities and mfp for two representative nanoribbons with $W/L \approx 0.43$ and 0.86. The calculations show that the corresponding exponents γ and ϵ do not depend of the aspect ratio, such that our results remain valid even for wide sheets with $W/L \sim 1$. This is not surprising because with the chosen parameters even ribbons with the small aspect ratio $W/L \ll 1$ support many propagating modes, i.e., they are essentially (quasi-)two dimensional.

Let us now use our results to discuss available experimental data. In experiments, the electron-density dependence of the mobility, $\mu=\mu(n)$, the conductivity, $\sigma=\sigma(n)$, and the mean-free path, $\text{mfp}=\text{mfp}(n)$ are accessible.[9,10] The dependencies [Eqs. (20)–(22)] can therefore be used to extract information about the transport regime for the system at hand. For example, for the mobility the exponent $\lambda=0.5$ would correspond to a purely ballistic transport regime, whereas $\lambda=0$ would describe a purely diffusive one. An intermediate exponent $0<\lambda<0.5$ would indicate the quasiballistic transport regime; the more close the value of λ to 0, the more diffusive the system is. Similar arguments applies to the conductivity (and mfp) where the corresponding exponent γ (and ϵ) lies between 0.5 and 1 (and between 0 to 0.5). For example, the mobility measured by Du *et al.*[10] corresponds to $\lambda=0.5$ suggesting a purely ballistic transport regime. The electron-density dependence of the mobility and conductivity in graphene ribbons was also studied by Tan *et al.*[8] and Bolotin *et al.*[9] The measured conductivity followed the sublinear behavior [Eq. (21)] with $\gamma<1$. Both groups attributed the deviation from the linear dependence to the effect of the short-range scattering. Taking into account that the mean-free path in the graphene device is comparable to the device dimension, we can provide an alternative interpretation of their findings arguing that the observed in Refs. 8 and 9 sublinear behavior represents a strong evidence of the quasiballistic transport regime.

IV. CONCLUSIONS

In the present study we perform numerical calculations of the conductance of graphene ribbons based on the Landauer

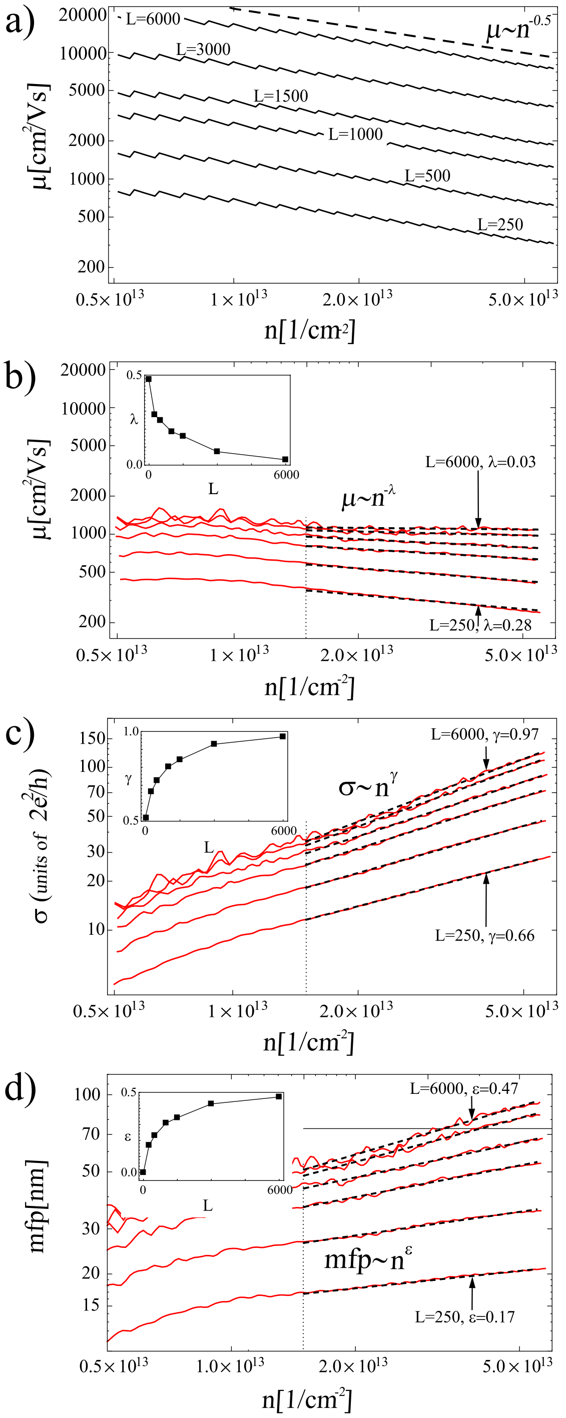

FIG. 9. (Color online) The mobility as a function of the electron density for (a) prefect zigzag nanoribbons and for (b) zigzag nanoribbons ribbon in the presence of charged impurities. The inset in (b) shows a dependence $\lambda=\lambda(L)$. (c) The conductivity and (d) the mfp as a function of the electron concentration for nanoribbons in the presence of charged impurities. The insets in (c) and (d) show the dependencies $\gamma=\gamma(L)$ and $\epsilon=\epsilon(L)$. The thin horizontal line in (d) marks the length of the longest ($L=6000$ sites) ribbon. The parameters of the ribbons and the impurity strength are the same as in Figs. 7 and 8. The dashed lines in (b) and (c) show the fits $\mu\sim\mu^{\lambda}$ and $\sigma\sim\sigma^{\gamma}$ for the electron densities $n\gtrsim 1.5\times 10^{13}$ cm^{-2} (as indicated by a vertical dotted line). The mobilities, conductivities, and mfps are averaged over ten impurity configurations.

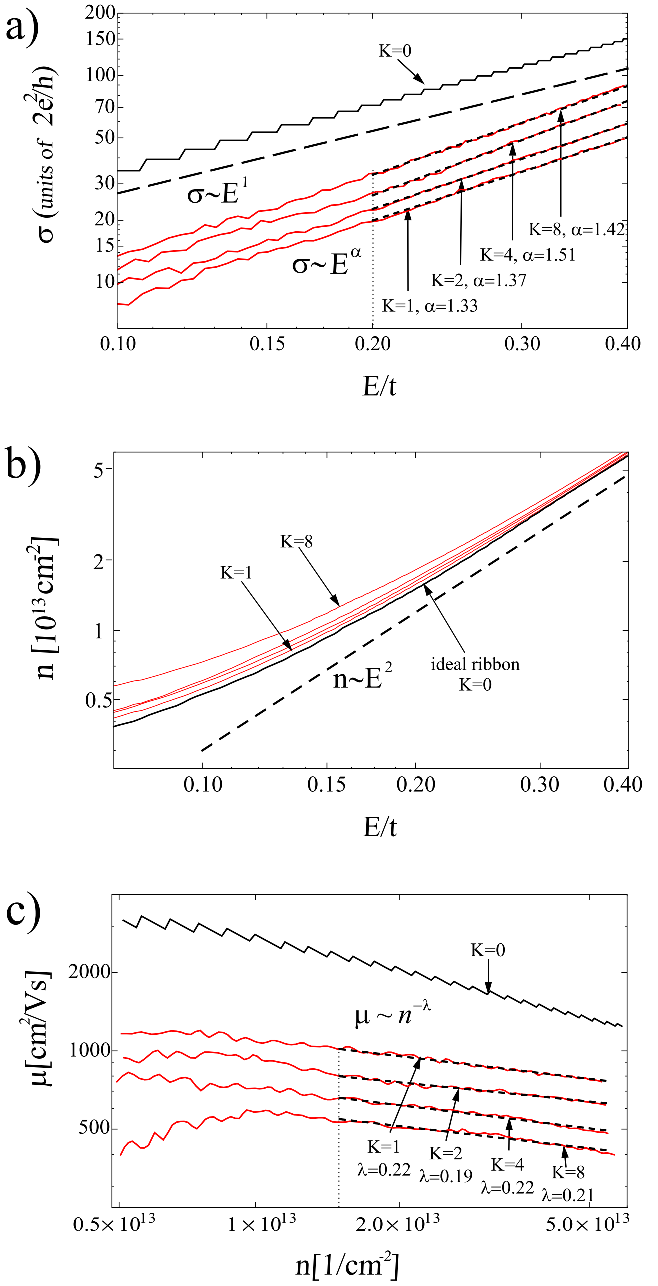

FIG. 10. (Color online) (a) The conductivity, (b) the electron density versus the Fermi energy, and (c) the mobility versus the electron density for graphene nanoribbon for different impurity strengths $K=1,2,4,8$, $\xi=4a$, and $n_{imp}=10^{12}$ cm^{-2}. The ribbon's dimension is $L\times W=123\times 53$ nm^2 (1000×250 sites). The dashed lines in (a) and (c) show the fits according to Eqs. (18) and (19) for, respectively, $E>0.2t$ and $n\gtrsim 1.5\times 10^{13}$ cm^{-2}. (The beginning of respective fitting intervals is indicated by vertical dotted lines). The conductivities are averaged over ten impurity configurations.

formalism and the tight-binding p-orbital Hamiltonian including the effect of warping of graphene and realistic long-range impurity potential. The effect of warping is included in our model by modification of the nearest-neighbor hopping integrals resulting from stretching/contraction of the surface and the π-σ rehybridization. We find that the modification of the nearest-neighbor hopping due to the warping of the

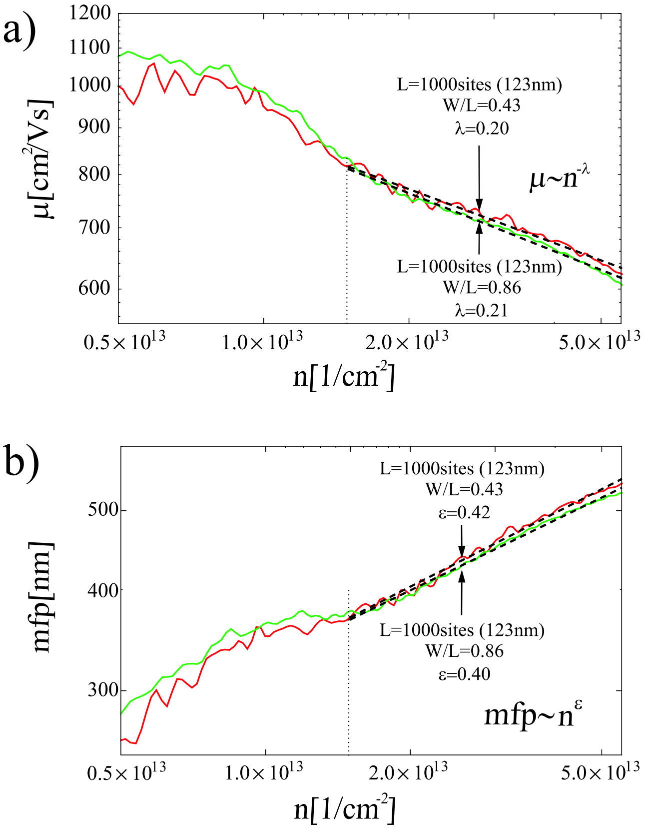

FIG. 11. (Color online) (a) The mobility and (b) the mfp of two representative nanoribbons with different widths $W=250$ sites (53 nm) and 500 sites (106 nm) (red and green curves correspondingly). The length is kept fixed $L=1000$ sites (123 nm) such that the aspect ratio W/L is equal 0.43 ($W=250$ sites), respectively, 0.86 ($W=500$ sites). The aspect ratio is expressed as the ratio of the actual dimensions of the ribbons (indicated in the figure in nanometer). (Note the number of sites per unit of length is different along and across the ribbon). We used the same strength and concentration of impurities as in Fig. 9. The calculations are averaged over ten impurity configurations.

graphene surface has a negligible effect on the conductance in comparison to the effect charged impurities even for moderate strength and concentration.

The main focus of our study is a transition from the ballistic to the diffusive transport regime in realistic graphene ribbons with long-range impurities which occurs as the size of the system increases. We keep in our study the width of the ribbon W constant and increase the ribbon length L, such that the diffusive regime is achieved when $L/W \gg 1$. We however show that the results presented in the paper remain valid even for wide sheets with $W/L \sim 1$.

We demonstrated that the conductivity of graphene ribbons follows a power-law dependence $\sigma \sim E^{\alpha}$ with $1 \leq \alpha \lesssim 2$. The case $\alpha=1$ corresponds to the ballistic regime whereas $\alpha=2$ corresponds to the diffusive regime which is reached for sufficiently long ribbons. In the ballistic regime the conductivity scales linearly with the length of the system L, whereas in the diffusive regime the conductivity saturates with L.

We find that the average electron density in the ribbons with impurities is practically not reduced in comparison to the ideal ribbons and follows the same quadratic dependence $n \sim E^2$ regardless of the transport regime (ballistic, quasiballistic, or diffusive). This behavior is consistent with the exponent $\alpha=2$ reached in the diffusive case because in this case the mobility $\mu=\sigma/en$ becomes independent on the energy (and hence on the electron density) as expected for the diffusive regime.

In experiments the electron-density dependence of the mobility, $\mu=\mu(n)$, is accessible. We find that the mobility of graphene ribbons varies as $\mu(n) \sim n^{-\lambda}$, with $0 \leq \lambda \lesssim 0.5$. The exponent λ depends on the size of the system with $\lambda=0.5$ corresponding to short ribbons in the ballistic regime, whereas the diffusive regime $\lambda=0$ (when the mobility is independent on the electron density) is reached for sufficiently long ribbons. Our results can be used for the interpretation of the experimental data when the value of the parameter λ can be used to distinguish the transport regime of the system (i.e., ballistic, quasiballistic, or diffusive). The corresponding electron-density dependence for the conductivity is $\sigma(n) \sim n^{-\gamma}$, where the exponent γ ranges from 1 in the diffusive limit to 0.5 in the ballistic limit. Based on our findings we discuss the available experiments and provide an alternative interpretation of some experimental conclusions.[8–10]

Our calculations also demonstrate that in the quasiballistic regime (which corresponds to many experimental studies) the mobility and the conductivity of the structure at hand strongly depend on the system size. Therefore in this regime the conductivity does not exist as a local property and the mobility cannot be considered as a well-defined material parameter because of its dependence on the system size. It should finally be noted that the possibly significant effect of warping-induced electrostatic potentials due to a modulation of the van der Waals force between the graphene and the substrate on the mobility is beyond the scope of the present paper and will be discussed in a separate work.

ACKNOWLEDGMENTS

J.W.K. was supported by the Polish Ministry of Science and Higher Education within the program *Support of International Mobility, 2nd edition*. A.A.S. and I.V.Z. acknowledge the support from the Swedish Research Council (VR), Swedish Institute (SI), and from the Swedish Foundation for International Cooperation in Research and Higher Education (STINT) within the DAAD-STINT collaborative grant. H.X. and T.H. acknowledge financial support from the German Academic Exchange Service (DAAD) within the DAAD-STINT collaborative grant.

APPENDIX: ELECTRON CONDUCTIVITY, MOBILITY, AND ELECTRON DENSITY IN THE BALLISTIC REGIME

In the low-energy limit close to the charge neutrality point $E=0$ the electron density of the zigzag graphene nanoribbon of the width N reads[48]

$$n(E) = \frac{4}{\pi\sqrt{3}} \frac{1}{t_0 a_0} \frac{1}{W} \sqrt{E^2 - E_m^2}\, \theta(|E| - |E_m|), \qquad \text{(A1)}$$

where the threshold energies have the form[49]

$$E_m = \frac{3\pi}{8} t_0 a_0 \frac{1}{W}\left(m + \frac{1}{2}\right), \quad m = 0,1,2,\ldots \tag{A2}$$

Noticing that the function $\sqrt{E^2 - E_m^2}$ approaches E for $E \gg E_m$ we can write the electron density in the approximate form

$$n(E) \approx \frac{4}{\pi\sqrt{3}} \frac{1}{t_0 a_0} \frac{1}{W} E \sum_m \theta(|E| - |E_m|). \tag{A3}$$

Summation of θ functions in Eq. (A3) gives a number of propagating modes at the given energy. Expressing this number with energy by making use of Eq. (A2) and approximating $E \approx E_m$ we obtain

$$n(E) \approx \frac{32}{\pi^2 3\sqrt{3}} \frac{1}{t_0^2 a_0^2} E^2. \tag{A4}$$

A comparison of the approximate expression (A4) with the exact one, Eq. (A1), is shown in Fig. 12(a).

In the low-energy limit close to the charge neutrality point $E=0$ the conductivity of the zigzag graphene nanoribbon of the width N reads[49]

$$\sigma(E) = \frac{2e^2}{h} \frac{L}{W}\left[\sum_m 2\theta(|E| - |E_m|) + 1\right]. \tag{A5}$$

Using similar approximations as above we obtain

$$\sigma(E) \approx \frac{2e^2}{h} \frac{16}{3\pi} \frac{1}{t_0 a_0} L|E|. \tag{A6}$$

Finally, substituting Eq. (A6) and (A4) into the definition of the mobility [Eq. (5)] and the mean-free path [Eq. (6)] we obtain

$$\mu = \frac{\sigma}{en} \approx \frac{e}{h} \pi\sqrt{3} t_0 a_0 L|E|^{-1} = \frac{e}{h} \frac{4\sqrt{2}}{\sqrt[4]{3}} L n^{-0.5} \tag{A7}$$

and

$$\mathrm{mfp} = \frac{h}{2e^2} \frac{\sigma}{\sqrt{\pi n}} = \frac{4}{\sqrt{2\pi\sqrt[4]{3}}} L. \tag{A8}$$

A comparison of the approximate expression for the conductivity, the mobility with the exact ones is shown in Figs. 12(b) and 12(c).

The above expression for $n(E)$, $\sigma(E)$, $\mu(n)$, and mfp are obtained for the zigzag ribbons. Corresponding expression for the armchair nanoribbons showing qualitatively the same dependence on E and n can be easily derived in a similar way utilizing the expression for the threshold energies E_m provided by Onipko.[49]

It should be noted that expressions (A1), (A3), and (A4) for the electron density n do not include a contribution from the edge states existing in the zigzag nanoribbons for the energies close to $E=0$. Because of this the electron density of the nanoribbon shown in Fig. 12 vanishes at $E=0$ and the mobility μ exhibits a singularity. Accounting for the contribution from the edge state in exact numerical calculations leads to the finite values of n and μ at $E=0$. However, for high energies sufficiently away the charge neutrality point this contribution does not practically affect n and μ, which justifies the utilization of expressions (A1)–(A7).

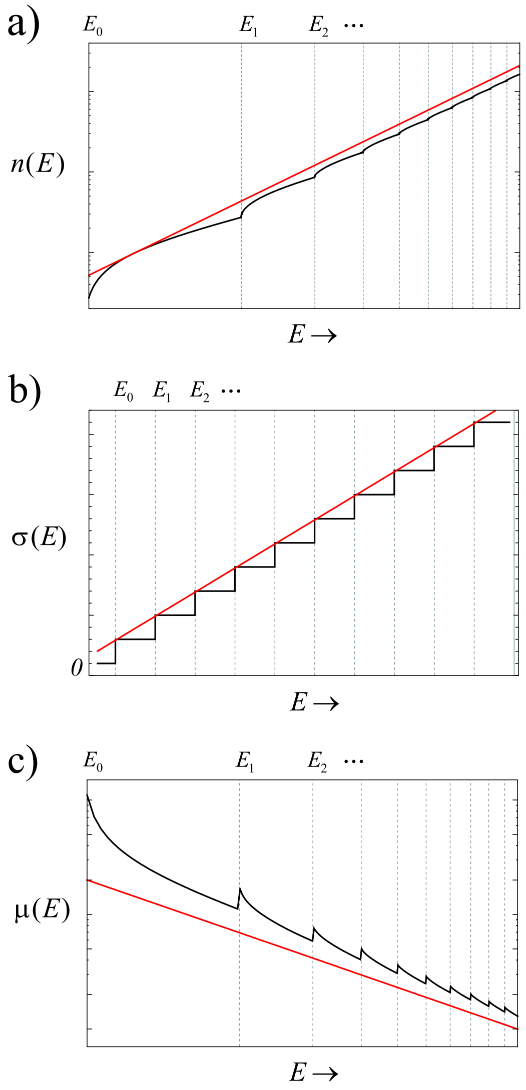

FIG. 12. (Color online) (a) The electron density, (b) the conductivity, and (c) the mobility as functions of the Fermi energy for a zigzag nanoribbon. Red lines correspond to the approximate expressions (A4), (A6), and (A7), whereas the black lines to the exact expressions (A1) and (A5).

*klos@amu.edu.pl

†igor.zozoulenko@itn.liu.se

[1] K. S. Novoselov, A. K. Geim, S. V. Morozov, D. Jiang, Y. Zhang, S. V. Dubonos, I. V. Grigorieva, and A. A. Firsov, Science **306**, 666 (2004).

[2] A. K. Geim and K. S. Novoselov, Nature Mater. **6**, 183 (2007); A. H. Castro Neto, F. Guinea, N. M. R. Peres, K. S. Novoselov, and A. K. Geim, Rev. Mod. Phys. **81**, 109 (2009).

[3] T. Ando, J. Phys. Soc. Jpn. **75**, 074716 (2006).

[4] K. Nomura and A. H. MacDonald, Phys. Rev. Lett. **96**, 256602 (2006).

[5] S. Adam, E. H. Hwang, V. M. Galitski, and S. Das Sarma, Proc. Natl. Acad. Sci. U.S.A. **104**, 18392 (2007).

[6] E. H. Hwang, S. Adam, and S. Das Sarma, Phys. Rev. Lett. **98**, 186806 (2007).

[7] K. Nomura and A. H. MacDonald, Phys. Rev. Lett. **98**, 076602 (2007).

[8] Y.-W. Tan, Y. Zhang, K. Bolotin, Y. Zhao, S. Adam, E. H. Hwang, S. Das Sarma, H. L. Stormer, and P. Kim, Phys. Rev. Lett. **99**, 246803 (2007).

[9] K. I. Bolotin, K. J. Sikes, Z. Jiang, M. Klima, G. Fudenberg, J. Hone, P. Kim, and H. L. Stormer, Solid State Commun. **146**, 351 (2008).

[10] X. Du, I. Skachko, A. Barker, and E. Y. Andrei, Nat. Nanotechnol. **3**, 491 (2008).

[11] J. C. Meyer, A. K. Geim, M. I. Katsnelson, K. S. Novoselov, T. J. Booth, and S. Roth, Nature (London) **446**, 60 (2007).

[12] A. Fasolino, J. H. Los, and M. I. Katsnelson, Nature Mater. **6**, 858 (2007).

[13] E.-A. Kim and A. H. Castro Neto, EPL **84**, 57007 (2008).

[14] M. I. Katsnelson and A. K. Geim, Philos. Trans. R. Soc. London, Ser. A **366**, 195 (2008).

[15] F. de Juan, A. Cortijo, and M. A. H. Vozmediano, Phys. Rev. B **76**, 165409 (2007).

[16] A. Isacsson, L. M. Jonsson, J. M. Kinaret, and M. Jonson, Phys. Rev. B **77**, 035423 (2008).

[17] V. Geringer, M. Liebmann, T. Echtermeyer, S. Runte, M. Schmidt, R. Rückamp, M. C. Lemme, and M. Morgenstern, Phys. Rev. Lett. **102**, 076102 (2009).

[18] A. Deshpande, W. Bao, F. Miao, C. N. Lau, and B. J. LeRoy, Phys. Rev. B **79**, 205411 (2009).

[19] J. Sabio, C. Seoánez, S. Fratini, F. Guinea, A. H. Castro Neto, and F. Sols, Phys. Rev. B **77**, 195409 (2008).

[20] F. Miao, S. Wijeratne, Y. Zhang, U. C. Coskun, W. Bao, and C. N. Lau, Science **317**, 1530 (2007).

[21] S. Russo, J. B. Oostinga, D. Wehenkel, H. B. Heersche, S. S. Sobhani, L. M. K. Vandersypen, and A. F. Morpurgo, Phys. Rev. B **77**, 085413 (2008).

[22] J. H. Bardarson, J. Tworzydlo, P. W. Brouwer, and C. W. J. Beenakker, Phys. Rev. Lett. **99**, 106801 (2007).

[23] A. Rycerz, J. Tworzyldo, and C. W. J. Beenakker, EPL **79**, 57003 (2007).

[24] D. A. Areshkin, D. Gunlycke, and C. T. White, Nano Lett. **7**, 204 (2007).

[25] E. Louis, J. A. Vergés, F. Guinea, and G. Chiappe, Phys. Rev. B **75**, 085440 (2007).

[26] D. Gunlycke, D. A. Areshkin, and C. T. White, Appl. Phys. Lett. **90**, 142104 (2007).

[27] T. C. Li and S.-P. Lu, Phys. Rev. B **77**, 085408 (2008).

[28] D. Querlioz, Y. Apertet, A. Valentin, K. Huet, A. Bournel, S. Galdin-Retailleau, and P. Dollfus, Appl. Phys. Lett. **92**, 042108 (2008).

[29] Y.-M. Lin, V. Perebeinos, Zh. Chen, and Ph. Avouris, Phys. Rev. B **78**, 161409(R) (2008).

[30] M. Evaldsson, I. V. Zozoulenko, H. Xu, and T. Heinzel, Phys. Rev. B **78**, 161407(R) (2008).

[31] C. H. Lewenkopf, E. R. Mucciolo, and A. H. Castro Neto, Phys. Rev. B **77**, 081410(R) (2008).

[32] E. R. Mucciolo, A. H. Castro Neto, and C. H. Lewenkopf, Phys. Rev. B **79**, 075407 (2009).

[33] H. Xu, T. Heinzel, and I. V. Zozoulenko, Phys. Rev. B **80**, 045308 (2009).

[34] E. Rossi and S. Das Sarma, Phys. Rev. Lett. **101**, 166803 (2008).

[35] P. Dietl, G. Metalidis, D. Golubev, P. San-Jose, E. Prada, H. Schomerus, and G. Schön, Phys. Rev. B **79**, 195413 (2009).

[36] Z. Chen, Y.-M. Lin, M. J. Rooks, and P. Avouris, Physica E (Amsterdam) **40**, 228 (2007).

[37] M. Y. Han, B. Ozyilmaz, Y. Zhang, and P. Kim, Phys. Rev. Lett. **98**, 206805 (2007).

[38] I. V. Zozoulenko, F. A. Maao, and E. H. Hauge, Phys. Rev. B **53**, 7975 (1996).

[39] H. Xu, T. Heinzel, M. Evaldsson, and I. V. Zozoulenko, Phys. Rev. B **77**, 245401 (2008).

[40] A. Hansson and S. Stafström, Phys. Rev. B **67**, 075406 (2003).

[41] R. S. Mulliken, C. A. Rieke, D. Orloff, and H. Orloff, J. Chem. Phys. **17**, 1248 (1949).

[42] L. D. Landau and E. M. Lifshitz, *Theory of Elasticity*, 3rd ed. (Pergamon, New York, 1986).

[43] *Statistical Mechanics of Membranes and Surfaces*, edited by D. R. Nelson, T. Piran, and S. Weinberg (World Scientific, Singapore, 2004).

[44] T. A. Witten, Rev. Mod. Phys. **79**, 643 (2007).

[45] J. Oprea, *Differential Geometry and Its Applications*, 2nd ed. (Pearson Prentice Hall, Upper Saddle River, New Jersey, 2004).

[46] S. Adam and S. Das Sarma, Phys. Rev. B **77**, 115436 (2008).

[47] P. W. Anderson, D. J. Thouless, E. Abrahams, and D. S. Fisher, Phys. Rev. B **22**, 3519 (1980); P. A. Lee and T. V. Ramakrishnan, Rev. Mod. Phys. **57**, 287 (1985).

[48] A. A. Shylau, J. W. Klos, and I. V. Zozoulenko, Phys. Rev. B **80**, 205402 (2009).

[49] A. Onipko, Phys. Rev. B **78**, 245412 (2008).